

Estimation of Influence of Target Material Type on Penetration Capability of 12.7 mm Armor-Piercing Projectile

Alan Catovic¹, Elvedin Kljuno¹

¹ *University of Sarajevo, Mechanical Engineering Faculty,
Vilsonovo setaliste 9, Sarajevo, Bosnia and Herzegovina*

Abstract – In the study an estimation of the influence of target material type on the penetration capability of the 12.7 mm API-T (armor-piercing incendiary with tracer) projectile is performed. The literature review contains 14 references regarding 12.7 mm ammunition studies. A relatively large number of metallic targets are taken into consideration in a computer simulation that assesses the influence of the target type on the penetration capabilities of the given projectile. By comparing the acquired findings with the data of other authors, the numerical model was first successfully validated. Simulation results indicate that bainitic steels are by far the most resilient steels. Because of their hardness, these steels displayed significant erosion of the penetrator tip and significant projectile fragmentation upon impact. Iron targets, as expected, performed worse than steel targets, with more penetration seen. Mild steel had a significantly deeper penetration compared to armor steel. The performance of other steels employed in the study was comparable. Numerical simulations have shown to be a very effective technique in ammunition and armor design, resulting in substantial time and cost savings (fewer experimental experiments). Furthermore, by utilizing simulations, researchers can estimate certain physical processes that would be challenging to detect in actual testing.

DOI: 10.18421/TEM134-01

<https://doi.org/10.18421/TEM134-01>


Corresponding author: Elvedin Kljuno,
*University of Sarajevo - Mechanical Engineering Faculty,
Vilsonovo setaliste 9, Sarajevo, Bosnia and Herzegovina.*
Email: kljuno@mef.unsa.ba

Received: 14 July 2024.

Revised: 30 October 2024.

Accepted: 04 November 2024.

Published: 27 November 2024.

 © 2024 Elvedin Kljuno & Alan Catovic ; published by UIKTEN. This work is licensed under the Creative Commons Attribution-NonCommercial-NoDeriv 4.0 License.

The article is published with Open Access at <https://www.temjournal.com/>

Keywords – Small-caliber ammunition, 12.7 mm projectile, penetration, terminal ballistics, simulation.

1. Introduction

The Warsaw Pact nations, including Russia, China, Iran, North Korea, and many more, utilize the 12.7×108 mm cartridge for heavy machine guns and anti-materiel rifles. Cartridge was developed in 1934 to provide one similar to the American .50 Browning Machine Gun round (12.7×99 mm NATO) and the German 13.2 mm TuF anti-tank rifle round. The 12.7×108 mm cartridge is a versatile munition that can be utilized against a broad range of targets in combat. It can destroy regular vehicles, perforate vehicles with light armor, and cause damage to external equipment such as searchlights, radar, transmitters, vision blocks, and engine compartment covers on heavily armored vehicles (like tanks). Moreover, it may ignite diesel fuel and, as of late, gasoline.

The ability to design such ammunition and assess its effectiveness on target is shortened by the use of numerical simulations. They not only speed up the ammunition design process but also significantly reduce design costs because they require fewer experimental tests and enable the optimization of the ammunition design process itself.

This study is divided into several sections: a review of the literature, a validation of the numerical model, and a section on numerical simulations with analysis and conclusions.

2. The Review of Research

Many studies on the penetrating capability of small-caliber ammunition of caliber 12.7 mm are available in public literature.

The performance of a perforated armor plate against a 12.7 mm AP-T projectile was examined (via experiments and numerical simulations) by Mubashar *et al.* [1].

They state that, in contrast to the projectile penetrating through a base aluminum plate without the perforated armour plate, the combination of the perforated (steel) and base armour (steel) plates was able to block the penetration of the armour piercing (AP) projectile.

By inclining the surface of the armour in relation to the projectile's initial axis, Zochowski [2] examined the prospect of boosting the efficiency of passive armour protection through testing and simulations. In the study, projectiles with calibers of 7.62 mm, 12.7 mm, and 14.5 mm were employed.

By combining rolled homogeneous armor steel base plate with non-homogenous spaced armor in the form of multilayer wire mesh, Balos *et al.* [3] attempted to improve the armor system's ballistic protection. It was discovered that variations in the wire body-to-body distance, some of which can increase and result in diminished contact with the projectile and insufficient yaw, have a detrimental influence on ballistic resistance caused by the tilt of the armor system. The vertical position is the ideal target inclination.

The effectiveness of Composite Metal Foam (CMF) armors against 0.50 caliber (12.7x99 mm, Ball and AP type) projectiles was estimated by Marx *et al.* [4]. A sandwich panel architecture including a thin aluminum back plate, a CMF core, and a ceramic faceplate was used to create a hard armor. With a mass efficiency of roughly 2.1 when compared to rolled homogeneous steel armor (RHA), CMF hard armors provide weight savings without compromising protection.

The defeat mechanisms offered by 4 mm thick slotted super-bainitic plates against hard-core 7.62x51 mm, AP, P80 bullets were examined by Frasa *et al.* [5]. They employed flash X-ray radiography and an ultra-high speed camera in experimental procedures, as well as numerical simulations.

In Wang *et al.* study [6], silicon carbide metal composite armors with the composite cover on the front of the SiC plate were subjected to 12.7 mm armor-piercing incendiary (API) projectiles. It was possible to determine the mass distributions of the fragments created when ceramic and projectile collided. After striking SiC/metal composite armor, the rigid-brittle core of the 12.7mm API projectile failed. This failure mechanism was investigated.

In comparison to monolithic plates with the same level of protection, Burian *et al.* [7] conducted both experimental and numerical studies showing that a well-designed hole pattern (in perforated plates made of contemporary ultra-high hardness nanostructured bainitic steel) can reduce the overall weight of the armour by as much as 40%.

The analyses were conducted using the 7.62 mm × 54R B-32 API and the 7.62×39 mm API BZ projectiles.

According to Gooch *et al.* [8], ATI 500-MILTM plate was developed, and after ballistic testing (V50 ballistic limits and standard deviation), it was added to the specification as Class 2 auto-tempered HHA steel. The projectiles examined were 14.5 mm B32, 0.30 cal APM2, 0.50 cal APM2, and 14.5 mm BS41.

Using computational analysis, Rahman *et al.* [9] examined the ballistic performance of magnesium alloy AZ31B, which served as the intermediate layer in a triple-layered laminated panel, and aluminum alloy Al7075-T6. A 7.62 mm armour-piercing projectile with a velocity range of 900-950 m/s was used to construct triple-layered panels using a commercial explicit finite element algorithm. Two models were built, the first of which used magnesium alloy as the intermediate layer and the second of which used aluminum alloy. Each model's ballistic performance was assessed in terms of penetration depth and ballistic limit velocity.

Through experiments and simulations, Kılıç *et al.* [10] looked into key mechanisms that prevent the high-hardness perforated plates from being penetrated by 7.62×54 mm armour-piercing projectile. Three mechanisms were found for defeating projectiles: the projectile core fracture, the projectile core nose erosion, and asymmetric pressures that cause the projectile to deviate from its intended trajectory.

In Wang *et al.* work [11], the ballistic performance of multi-layered, relatively thick metallic targets is examined when they are hit by 12.7-mm projectiles. The penetration process of each target has been simulated using the numerical method. The numerical results show that the ballistic performance of targets is significantly influenced by petal formation and friction.

Giglio *et al.* [12] created a FE (finite element) model of the impact of a NATO 7.62 mm projectile on an aluminum target using a numerical method. The impact of a material calibration on a soft-core projectile's mechanical characteristics has been assessed.

A constitutive strength and failure model for the steel core of a 14.5 mm API projectile was created by Paris *et al.* [13]. LS-DYNA was used to model the ballistic tests numerically.

The constitutive behavior of armor-piercing incendiary projectile (API) material and Armox 500T steel under varied stress states, strain rates, and temperatures was studied by Iqbal *et al.* [14].

Through numerical simulation of the high strain rate tension tests conducted on split Hopkinson pressure bar apparatus, the calibrated JC model for Armox 500T steel has been validated. Armox 500T steel target plates with thicknesses of 8 and 10 mm were used for the experiments. 7.62 and 12.7 API rounds struck them at a normal incident angle. Finite element simulations using a calibrated JC model for both the projectile material and the target were used to replicate the tests.

3. Numerical Simulations

In this part, numerical simulations will be performed, regarding the 12.7 mm API-T projectile.

3.1. Introduction

The study's simulations were made in Autodyn Lagrange processor from Ansys Workbench. Time-dependent problems including geometric and material nonlinearities can be solved by the hydrocode Autodyn using finite-element, finite-difference, and finite-volume approaches. The Lagrange processor often employs a structured (I-J-K) numerical mesh made up of brick components (3D) or quadrilaterals (2D). The vertices of the mesh follow the rate of material flow in lockstep.

Compared to the Eulerian technique, the Lagrange formulation is computationally quicker since it does not need the computation of material movement over the mesh. Free surfaces, material interfaces, and history-dependent material behavior may all be better understood using the Lagrange framework. The primary disadvantage of the Lagrange approach is that excessive material movement might seriously deform the numerical mesh, which could result in an insufficient solution, and the calculation stops.

One way to fix mesh distortion is to „rezone“ the mesh, which is projecting the distorted solution into the normal mesh.

Furthermore, Autodyn provides further methods, such as erosion, to extend the Lagrange formulation to highly deformed phenomena. The partial differential equations that must be solved in the Lagrange processor express the conservation of mass, momentum, and energy in Lagrangian coordinates. These outline the problem's solution coupled with a material model and a set of initial and boundary conditions [15].

3.2. The Numerical Model Validation

The validation of the 2D numerical model was first performed, using available data [1] where the residual velocity of 12.7 mm API-T (armor piercing incendiary with tracer) projectile (Figure 1), after perforating an aluminum alloy plate, was estimated using numerical simulations and analytical data. Dimensions of projectile parts and targets were also taken from [1]. The projectile in the simulation consisted of a hardened steel penetrator and brass casing, while the target was from high-strength aluminum alloy 5083-H116 (Mg content 4-4.9% by weight). AA5083-H116 is among the highest-strength aluminum-magnesium alloys. This alloy is commonly employed in marine applications and protective structures [1]. This alloy has moderate tensile strength (317 MPa) and hardness (85 HB), and extremely strong corrosion resistance (albeit it can deteriorate with extended exposure to high temperatures). Elongation at break is 16%, with a shear strength of 190 MPa. A benefit is that it can be welded. The melting temperature is 591-638 °C. It is used in gas/oil pipes, drilling rigs, pressure vessels, ordnance, and armor plates [27].

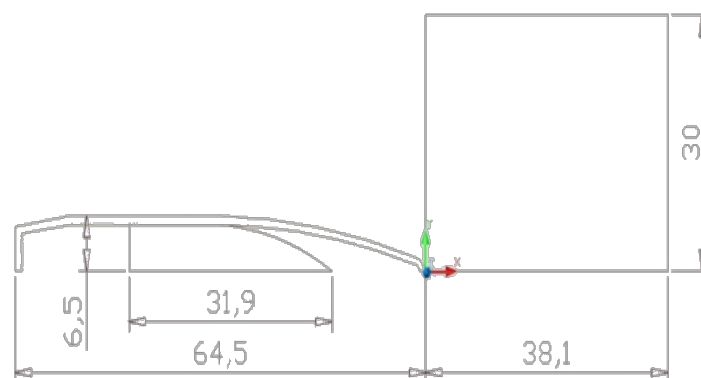


Figure 1. Dimensions of projectile (12.7 mm API-T) and target (2D axisymmetric model)

Total number of mesh elements in this case was 55220 (Figure 2). The initial condition was a projectile (impact) velocity of 864 m/s, as in [1].

The boundary condition was fixing the target on its outer edge (parallel to the symmetry axis).

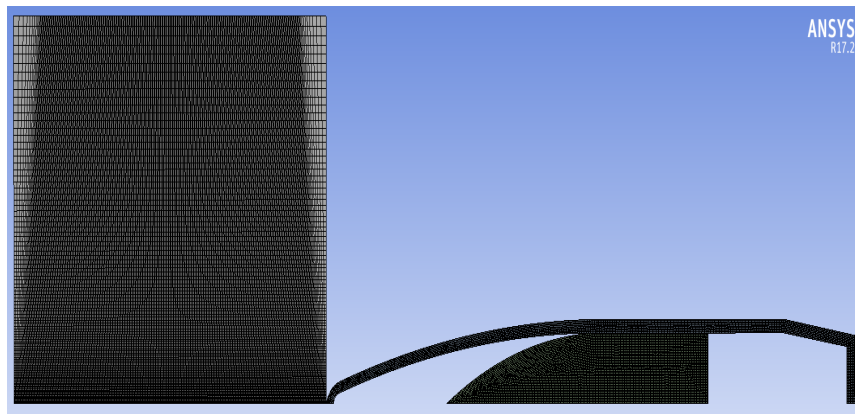


Figure 2. Mesh (0.1 mm) for projectile and target 2D axisymmetric model

Material models for the target and projectile parts (core and casing/gilding metal jacket), used in the simulation, were taken also from [1]. The Gruneisen shock equation of state [1] (Table 1) was used throughout, as well as the Johnson-Cook plasticity model [1] (Table 2). For this model, several constants are used: A (initial yield stress), B (strain hardening constant), n (strain hardening exponent), C (strain rate constant), and m (thermal softening constant). For material failure, the Johnson-Cook [1] failure model (table 3) was used, only for a target.

Erosion of elements was controlled by material failure and default geometric strain limit (1.5). The inertia of eroded elements was retained throughout the simulation.

The time of this simulation was taken as 200 μ s since during this timeframe projectile completely perforates this type of target. The time step safety factor was taken as the default value (0.9).

The result of the simulation can be seen in Figure 3. In the paper by Mubashar *et al.* [1], it is obtained for a given projectile and target that the residual velocity (after exiting the target) was 514.3 m/s using simulation, and 513.93 m/s using the analytical model of Forrestal *et al.* [33] In the simulation, the residual velocity of the projectile (lower part of the penetrator taken into account) is 512.38 m/s, which equates to a maximum relative error of 0.4% compared to results from the work presented in [1].

Table 1. Gruneisen shock EOS data for all components material

Material	Density (g/cm ³)	Gruneisen coefficient	c ₀ (m/s)	s
Casing (Brass) [1]	8.96	1.99	3940	1.48
Penetrator (Steel) [1]	7.85	1.93	4570	1.49
Target (AA 5083-H116) [1]	2.70	1.97	5340	1.40

Table 2. The constitutive Johnson-Cook model for all materials

Material	A (MPa)	B (MPa)	n	C	m
Casing (Brass) [1]	90	628	0.7201	0.2659	1
Penetrator (Steel) [1]	1900	1100	0.3	0.05	1
Target (AA 5083-H116) [1]	167	596	0.551	0.001	0.859

Table 3. Constants for the Johnson-Cook failure model for target material

Material	D ₁	D ₂	D ₃	D ₄	D ₅
Target (AA 5083-H116) [1]	0.0261	0.263	-0.349	0.147	16.8

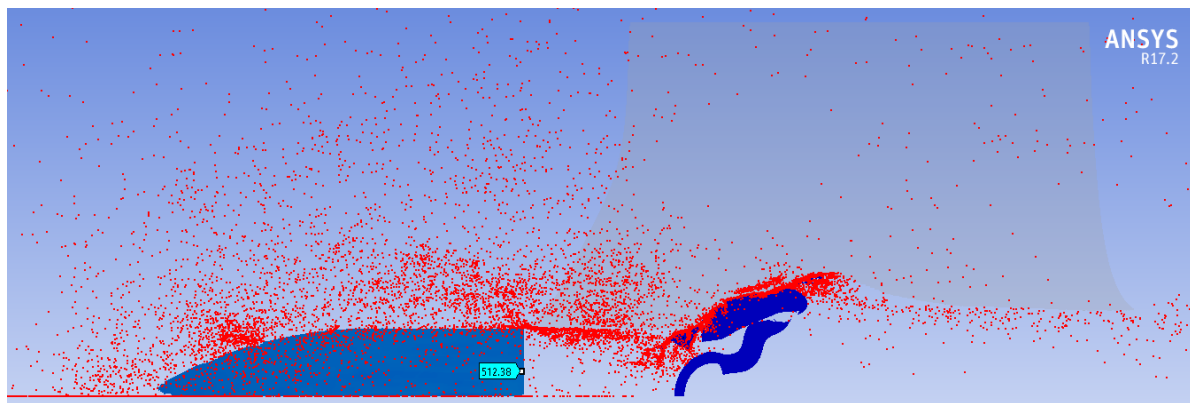


Figure 3. Result of validation simulation (2D axisymmetric): residual velocity (512.38 m/s) of a steel penetrator of 12.7 mm API-T projectile (brass case is visibly deformed)

3.3. Research of the Influence of Different Target Materials on Penetration Capability

The influence of different metallic target materials on the penetration capability of the 12.7 mm API-T projectile (presented with dimensions in Figure 1) was performed using the Ansys Autodyn program. Several 2D axisymmetric numerical simulations were performed with all parameters being the same as in the validation procedure (mesh, initial and boundary conditions, etc.), except that here different metallic target materials were used.

The time of simulations was taken as 200 μ s or 300 μ s, depending on the time needed for the projectile to perforate (aluminum target) or „settle“ in the target (steel and titanium targets). Parameters (EoS, plasticity model, and failure model) of several target materials (used in simulations) are presented in Tables 4 and 5. It is assumed that the EoS of state for all steels is the same. Brief theoretical explanations of these material models can be found in [1]. The section below covers characteristics of target materials used in simulations.

Aluminum alloy 2024-T3 consists of 4.76% Cu, 1.38% Mg, 0.65% Mn, 0.22% Fe, and other elements in small quantities (Si, Zn, Ti, Cr). Yield strength is 330 MPa, ultimate tensile strength is 477 MPa, and elongation 18.2% [16]. The hardness of the alloy is around 120 HB (Brinell).

This alloy is a high-strength material with sufficient workability, good machinability, and surface finish capabilities.

It is utilized in aircraft fittings, gears and shafts, fastening devices, rectifier parts, couplings, fuse parts, hydraulic valve bodies, computer parts, clock parts, ammunition, nuts, pistons, and gears [31].

Constitutive and failure model parameters for this alloy are taken from [16].

Alpha-beta titanium alloy Ti-6Al-4V has outstanding corrosion resistance and high specific strength. One of the most widely used titanium alloys, it is used in a variety of industries and biomechanical applications where low density and superior corrosion resistance are essential. With its density of 4.45 g/cm³, fracture toughness of 84-107 MPam^{1/2}, hardness of 300-500 HB, and tensile strength of 900-1300 MPa [25], [26], [27], [28], [29], titanium/aluminum/vanadium alloy has strategic military significance. Its characteristics are comparable to those of RHA with a comparable hardness. It can also be heat-treated and welded.

Titanium alloy plates of ballistic quality cost ten to twenty times as much as steel. Titanium alloy armor has been utilized in several applications, including as the M2 Bradley AFV's commander's hatch and upper armour protection, as well as in certain armored parts of the M1A2 Abrams MBT. It has also been utilized to lighten the 155 mm M777 howitzer. Applique constructions have, therefore, employed titanium alloy plates.

Titanium was also used in the building of the Mobile Tactical Light Vehicle, which was manufactured for the Canadian Army, to offer protection against 14.5-mm AP rounds. MIL-DTL-46077G provides specifications for ballistic limit data for testing [25].

Constitutive and failure model data for the Ti-6Al-4V alloy, used in numerical simulations, are taken from [16].

Table 4. Gruneisen shock EOS data for target materials

Material	Density (g/cm ³)	Gruneisen coefficient	c ₀ (m/s)	s
Steel/iron [1]	7.85	1.93	4570	1.49
Aluminum alloy 2024-T3 [16]	2.77	2.0	5328	1.34
Titanium alloy Ti6Al4V [16]	4.42	1.23	5130	1.03

Table 5. The constitutive Johnson-Cook model for different target materials

Material	A (MPa)	B (MPa)	n	C	m
Aluminum alloy 2024-T3 [16]	369	684	0.73	0.0083	1.7
Titanium alloy Ti-6Al-4V [16]	1098	1092	0.93	0.014	1.1
Iron Armco [Autodyn library]	175	380	0.32	0.06	0.55
Mild steel [19]	304	422	0.345	0.0156	0.87
RHA steel [20]	1193	500	0.676	0.00435	1.17
Armour steel [26]	980	2000	0.83	0.0026	1.4
Weldox 460 E steel [28,36]	490	383	0.45	0.0114	0.94
Weldox 700 E steel [17]	859	329	0.579	0.0115	1.071
Weldox 900 E steel [17]	992	364	0.568	0.0087	1.131
Steel 4340 [Autodyn library]	792	510	0.26	0.014	1.03
Steel Tenax [18]	1440	492	0.24	0.011	1.03
Steel 2P [18]	1210	773	0.26	0.014	1.03
Steel Armox 500T [1]	1372.5	835	0.2467	0.0617	0.84
Bainite steel [21]	1517	1575	0.35	0.01	1
Nanos-BA steel [20]	1303	1420	0.195	0.075	1.17

Iron Armco, whose constitutive and failure models can be found in the Ansys Autodyn library, is a pure, soft, durable material with high magnetic saturation, strong electric conductivity, low coercive force, and high corrosion resistance. It was created by the American Rolling Mill Company (ARMCO) in 1909. With a Fe percentage of 99.8–99.9% and a low carbon level, this is technically pure iron. In electric furnaces (mostly vacuum furnaces), it is utilized as a melting material to create low-carbon, non-corroding, non-magnetic, or heat-resistant cast steel [34].

Mild steel, reported in [19], consists of the following alloying elements: 0.188% C, 0.1855% Si, 0.8375% Mn, 0.0342% S, 0.0213% Cr, 0.0217% Ni, and 0.0762% Al. Calibration of constants for constitutive and failure models for this steel is also given in [19].

For almost a century, rolled homogeneous armour (RHA) has been widely utilized as an armor material. It is typically used as the standard for evaluating armour materials in depth-of-penetration tests. RHA is made by quenching and tempering steel ingots with a small amount of alloying elements, then hot-rolling the resulting ingots to create a through-hardened, tempered martensitic structure.

The general chemical composition of the RHA plate is: (0.18-0.32 C, 0.60-1.50 Mn, 0.05-0.95 Ni, 0.00-0.90 Cr, 0.30-0.60 Mo, 0.015 max. S and P).

The precise composition would be determined by the necessary characteristics and the thickness of the plate that has to be hardened [25].

Steel suppliers are often given flexibility by military standards to meet the necessary armour mechanical characteristics and ballistic requirements across a wide variety of chemical and treatment conditions.

The following is a common protocol for treating the RHA plate. The plate is typically quenched in water or oil and heated to a temperature between 820 °C and 860 °C to solidify the steel after it has been rolled into form. Because of the hard and brittle martensite phase's, the final product is extremely strong yet brittle. Tempering, which involves reheating the steel to temperatures between 400 °C and 650 °C in a furnace for a few hours, helps mitigate this. As a result of its homogenous microstructure and relative ductility and toughness, the finished product is referred to as homogeneous. With lower temperatures being utilized for the thinner, harder armour and higher temperatures for the thicker, tougher armour plate, the tempering temperature will be chosen to produce the desired mechanical and ballistic qualities [25].

Constitutive and failure model parameters for RHA can be found in [20].

Armour steel of unknown tradename is reported in [26].

Constitutive and failure model parameters for this steel can be found in the mentioned reference. The armour steel that the authors examined in [26] is a medium carbon, low alloy steel that was made from an armour plate that was 50 mm thick. To achieve a tempered martensite structure and guarantee an exceptional blend of high strength and ductility, the plate is hot rolled and heat treated.

Weldox is a high-strength steel that has excellent weldability, high ductility, and strength (numbers represent the nominal yield strength) altogether. This combination is achieved by applying heat treatment and rolling under strict control. The three alloys are treated differently. The high strength of TM steel Weldox 460 E is achieved through controlled cooling after rolling at a specific temperature. TM steels have a microstructure with less pearlite than normalized steel. Among the materials in this group that undergo a major quenching and tempering process are Weldox 700 E and Weldox 900 E.

Weldox 700 E and Weldox 900 E are composed of tempered martensite, whereas Weldox 460 E has a ferrite-pearlitic structure. Weldox 460 E's pearlite reduces strength while making the material extremely ductile. Layers of the dark pearlite can be seen in between ferrite grains. Constitutive and failure model parameters for Weldox 460 E steel are taken from [28], [32].

Weldox 700 E and Weldox 900 E's martensite shows both high strength and high brittleness. The tempering process has been applied to the martensite to increase its ductility in the alloys [17]. Constitutive and failure model parameters for Weldox 700 E and Weldox 900 E steels are taken from [17].

Steel 4340 is a medium-carbon, low-alloy steel. Compared to other steels, 4340 steel has excellent strength, ductility, toughness, creep resistance, and fatigue resistance. Yield strength of 470 MPa, tensile strength of 745 MPa, elongations (at break) of 22%, and hardness of 217 HB (can be hardened by cold working or heat treatment) are typical values for this steel [30].

Steel 4340 is used in power transmission gears and shafts, aircraft landing gear, and other structural parts. Constitutive and failure model parameters for steel 4340 can be found in Autodyn material library.

Steels under the names Tenax (tool steel) and 2P (armor steel) are reported in [18]. The chemical composition of these steels are as follows. Tenax steel: 0.68 C, 0.43 Mn, 0.65 Si, 0.019 P, 0.014 S, 1.28 Cr, 2.05 W, 0.16 V and 0.01 Ti. 2P steel: 0.28 C, 1.25 Mn, 1.45 Si, 0.016 P, 0.006 S, 0.22 Cr, 0.81 Ni, and 0.25 Mo. No mechanical characteristics for these steels are reported. Constitutive and failure model parameters are also given in [18].

Armox 500T is modern armour steel, manufactured by SAAB (Sweden). Armox 500T steel's great strength and high hardness make it appropriate for use in military and civil ballistic applications. The chemical composition of the material and calibration of Armox 500T steel (for obtaining the material parameters of the Johnson-Cook model) are given in [23], [24].

Mechanical properties for this steel are specified with a minimum yield strength of 1250 MPa, tensile strength of 1450-1700 MPa, and hardness in the range of 480-540 HB [24]. Constitutive and failure model parameters for this steel are taken from [1].

Depending on the alloy composition, steels can develop the plate-like microstructure known as bainite at temperatures between 125 and 550 °C. It is one of the products that can occur when austenite is cooled to the point at which it is no longer thermodynamically stable with regard to ferrite, cementite, or ferrite and cementite. It was first reported by Davenport and Bain.

Common constituents of bainite, a thin non-lamellar structure, include dislocation-rich ferrite and cementite. This ferrite is harder than it typically would be due to the high density of dislocations in the ferrite seen in bainite and the small size of the platelets in bainite. In contrast to martensitic steels, alloys based on bainite frequently don't require additional heat treatment upon transformation to maximize their toughness and strength.

Regarding bainitic steel (such as Nanos-BA), armor manufacturers are in recent times drawn to super-bainite (particularly for add-on armour) due to its exceptional blend of strength, hardness, and ductility. The mass of tested armor, needed to combat the same threats, divided by the mass of rolled homogeneous armour (RHA) is known as the ballistic mass efficiency (BME).

The BME of super-bainite armor is higher than that of titanium armor and is similar to that of alumina. Although the bainite structure is extremely hard, it is also relatively brittle. Super-bainite's high hardness is obtained by heat-treatment procedures that cause its grains to shrink by about 100 times in comparison to regular bainite. The thickness of fine bainitic ferrite plates is measured in tens of nanometers, which is significant since the strength of these structures is inversely correlated with the thickness of bainitic ferrite plates. The material acquires its ultra-high strength without the brittleness of bainite following the heat treatment and additives.

A hardness of 400 HB is required for conventional steel armor, such as rolled homogenized armour (RHA) steel. Super-bainite is tougher than 30-40 MPam^{1/2}, has a hardness of 600-670 HV, and its maximum tensile strength is around 2500 MPa [20].

Modern ultra-high hardness (UHH) nanostructured bainitic steel (i.e. super-bainitic Pavise™ SBS 600, UHH martensitic Mars® 300 steels) are described in [22]. In an arc furnace, steel ingots (of the following chemical composition: 0.55 C, 2.0 Mn, 1.8 Si, 1.37 Cr, 0.7 Mo, 0.11 V; wt. %) are melted; after that they are homogenized for 24 hours at 1200°C, and then hot forged into bars. The bars are then hot rolled to produce the various plate thicknesses. Austenitization is the first step in the steel's heat treatment procedure, which is then carefully cooled to the temperature of the isothermal

transition. For 120 hours, transformation to lower bainite is carried out at 210°C. The ideal blend of strength, toughness, and ductility of material can be achieved by optimizing the steel's chemical composition and heat treatment characteristics [22].

Results of simulations, namely the penetration process of 12.7 mm API-T projectile through different targets, with an assumed impact velocity of 864 m/s, are presented in Figure 4 (a-d).

Penetration depths into a given target for 12.7 mm API-T projectile, obtained in numerical simulations, are presented in Table 6.

Table 6. Penetration of 12.7 mm API-T projectile, obtained in simulations with the same impact velocity (864 m/s)

Target type	Penetration depth
Aluminum alloy 2024-T3 [16]	38 mm
Titanium alloy Ti-6Al-4V [16]	26.8 mm
Iron Armco [Autodyn library]	38 mm
Mild steel [19]	28.5 mm
RHA steel [20]	13.6 mm
Armour steel [26]	15.1 mm
Weldox 460 E steel [28]	25mm
Weldox 700 E steel [17]	17.1 mm
Weldox 900 E steel [17]	14.4 mm
Steel 4340 [Autodyn library]	17.7 mm
Steel Tenax [18]	9.5 mm
Steel 2P [18]	10.1 mm
Steel Armox 500T [1]	6.9 mm
Bainite steel [21]	6.4 mm
Nanos-BA steel [20]	4.2 mm

Figures 4 (a-d) and Table 6 show that the most resistant steels proved to be bainitic steels (i.e. Nanos-BA bainite steel), followed by Armox 500T steel.

These steels also showed large erosion of penetrator tip and largest fragmentation of projectile upon impact which is understandable since they are very hard steels.

Perforation was recorded for Aluminum alloy 2024-T3, as previously for AA5083-H116 (section 3.2, validation process).

Iron Armco performed as expected, with higher penetration observed (projectile stuck in target; short of perforation) than steel targets.

For baseline RHA steel depth of penetration observed for this projectile (and this impact velocity) was 13.6 mm.

Mild steel [19] showed higher penetration depth than armor steel which was also expected.

It must also be mentioned that Weldox 460 E steel [28] showed somewhat higher penetration depth comparing to armor steels. Other steels exhibited similar performance with recorded penetration depth ranging from 9.5 mm (Tenax steel) to 17.7 mm (steel 4340).

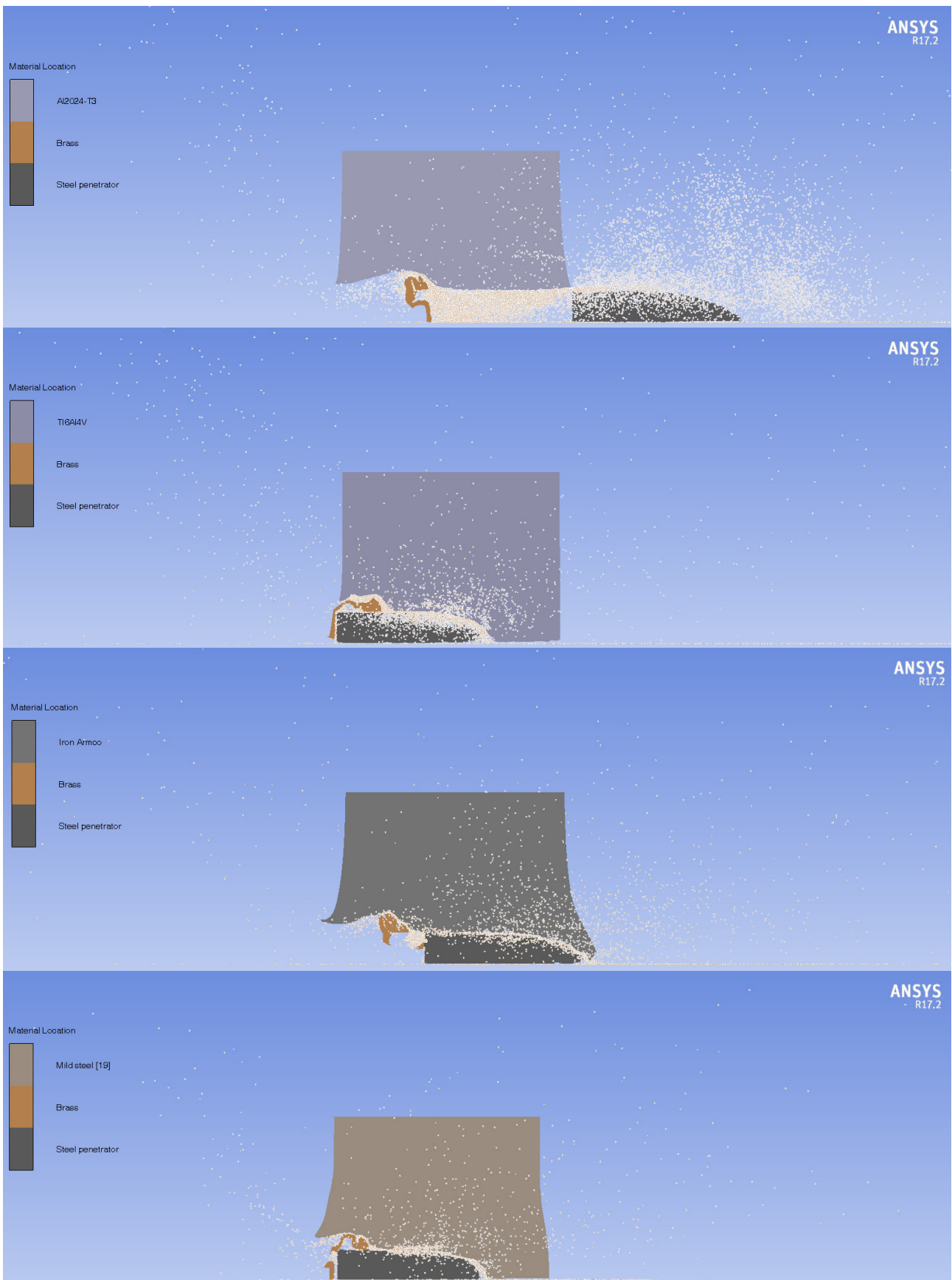


Figure 4a. Results of simulations: penetration process of 12.7 mm API-T projectile (steel penetrator and brass case) through different targets (assumed impact velocity: 864 m/s)

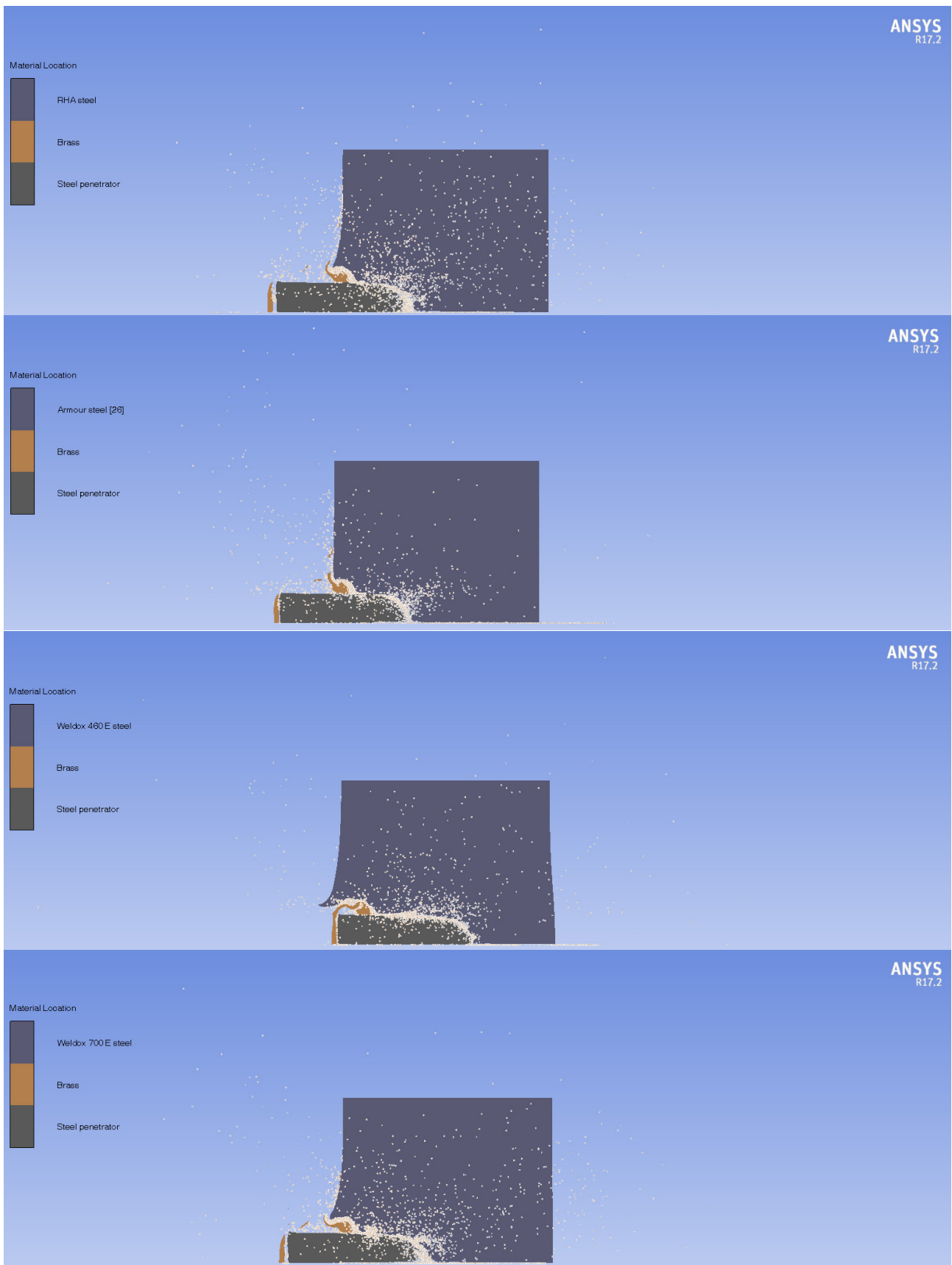


Figure. 4b. Results of simulations: penetration process of 12.7 mm API-T projectile (steel penetrator and brass case) through different targets (assumed impact velocity: 864 m/s)

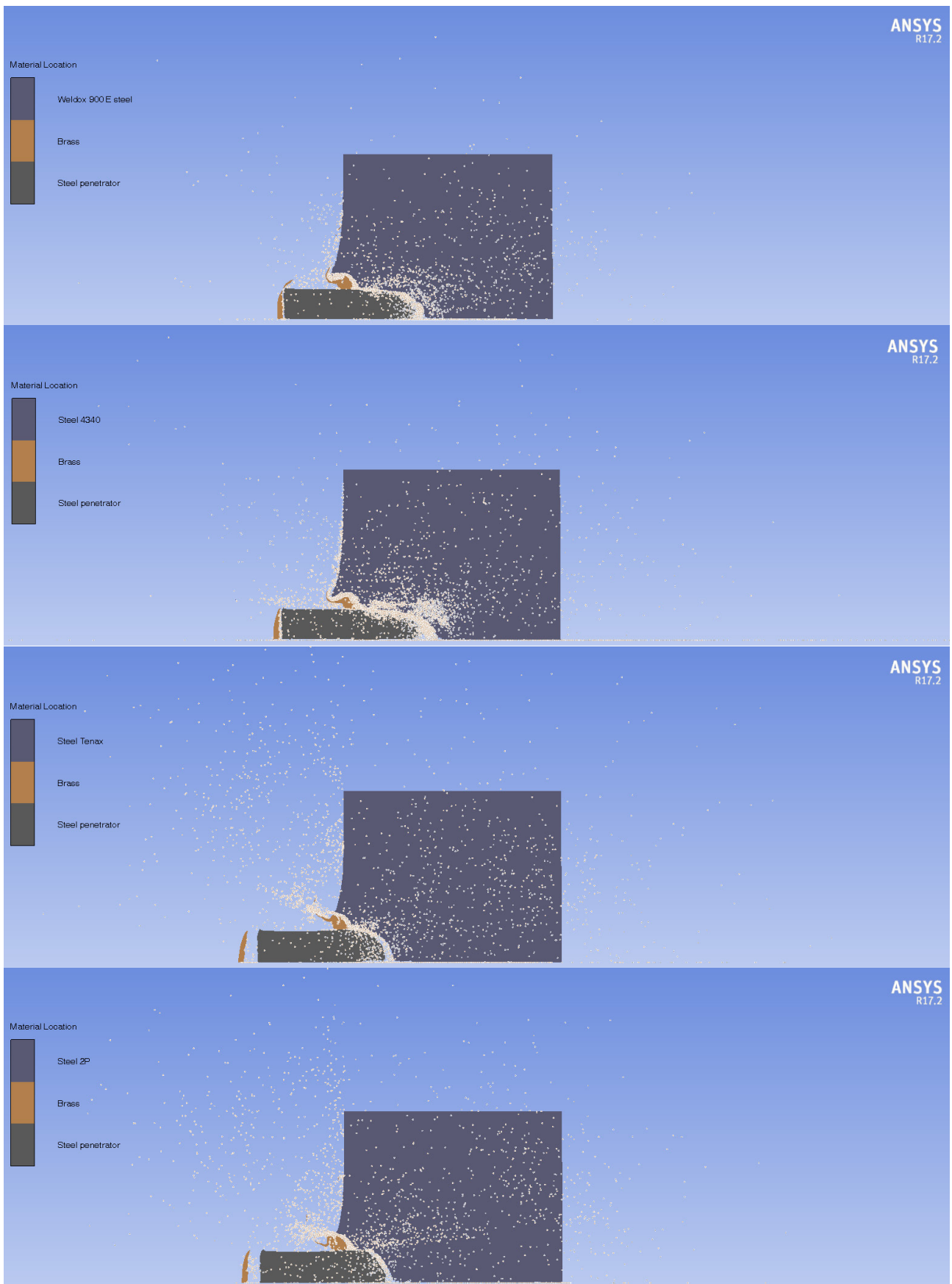


Figure 4c. Results of simulations: penetration process of 12.7 mm API-T projectile (steel penetrator and brass case) through different targets (assumed impact velocity: 864 m/s)

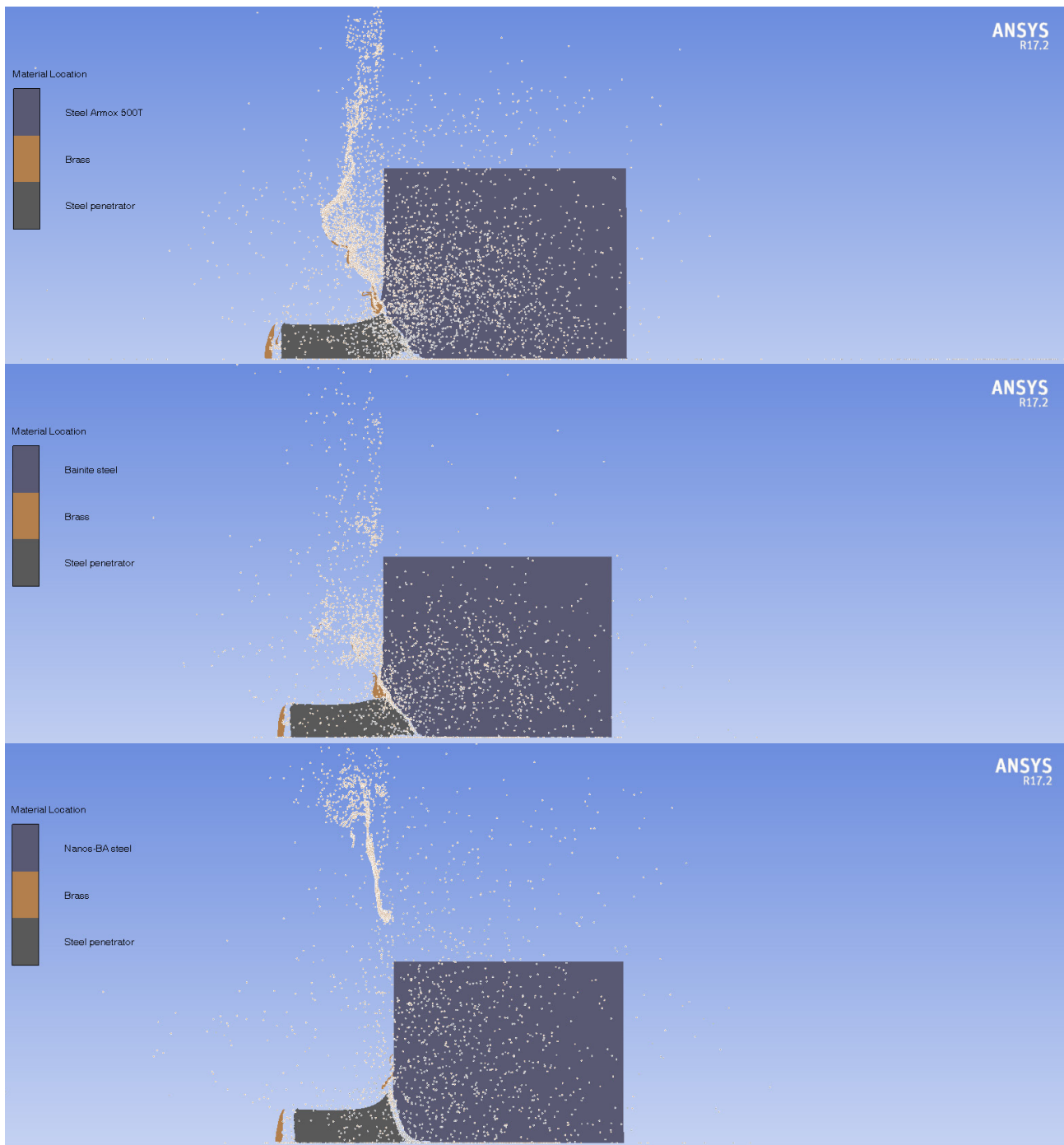


Figure 4d. Results of simulations: penetration process of 12.7 mm API-T projectile (steel penetrator and brass case) through different targets (assumed impact velocity: 864 m/s)

4. Conclusions

In the paper, analysis is performed with a 12.7 mm projectile, API-T (armor piercing incendiary tracer). The influence of the type of target on projectile efficiency was evaluated using numerical simulations, where several metallic targets were considered. Before the aforementioned analyses, the numerical model was successfully validated, comparing the obtained results with the data of other authors [1].

Results of simulations show that, as expected, the most resistant steels proved to be bainitic steels. These steels also showed large erosion of penetrator tip and the largest fragmentation of projectile upon impact because of their high hardness. Iron performed as expected, with higher penetration observed than steel targets. Mild steel showed significantly higher penetration depth than in the case of armor steels but lower than iron targets. Other steels exhibited similar performance with recorded penetration depth ranging from 9.5 mm to 17.7 mm.

It has been shown that numerical simulations can be a very powerful tool in ammunition design and can significantly save time and money in the process (fewer experimental tests). In addition, using simulations, one can predict (and try to explain) certain physical processes that would be difficult to identify in real tests (i.e. using high-speed cameras). Future work can be focused on 3D analysis, for different target obliquity, as well as for different target structures (i.e., different constructions of the perforated plate in front of the main armor). It must be noted, however, that 3D analysis (numerical explicit dynamics) requires high-performance computers (cluster of large number of processors).

References:

- [1]. Mubashar, A., *et al.* (2019). Ballistic response of 12.7 mm armour piercing projectile against perforated armour developed from structural steel. *Proceedings of the Institution of Mechanical Engineers, Part L: Journal of Materials: Design and Applications*, 233(10), 1993-2005.
- [2]. Zochowski, P. (2013). Add-on passive armour for light armoured vehicles protection, *Military Institute of Armament Technology*, 42.
- [3]. Baloš, S., Pećanac, M., Trivković, M., & Šidjanin, L. (2019). Ballistic behavior of multilayer wire mesh application armor. *Advanced Technologies and Materials*, 44(2).
- [4]. Marx, J., Portanova, M., & Rabiei, A. (2019). Ballistic performance of composite metal foam against large caliber threats. *Composite structures*, 225, 111032.
- [5]. Fras, T., Murzyn, A., & Pawlowski, P. (2017). Defeat mechanisms provided by slotted add-on bainitic plates against small-calibre 7.62 mm× 51 AP projectiles. *International Journal of Impact Engineering*, 103, 241-253.
- [6]. Wang, X., Yu, Y., Zhong, K., Jiang, Z., & Gao, G. (2021). Effects of impact velocity on the dynamic fragmentation of rigid-brittle projectiles and ceramic composite armors. *Latin American Journal of Solids and Structures*, 18(8), e410.
- [7]. Burian, W., Zochowski, P., Gmitrzuk, M., Marcisz, J., Starczewski, L., Juszczak, B., & Magier, M. (2019). Protection effectiveness of perforated plates made of high strength steel. *International Journal of Impact Engineering*, 126, 27-39.
- [8]. Gooch, W., Showalter, D., Burkins, M., Montgomery, J., & Squillacioti, R. (2009). Development and ballistic testing of a new class of auto-tempered high hard steels under military specification MIL-DTL-46100E. *Army research laboratory*.
- [9]. Rahman, N. A., *et al.* (2017). Characterising ballistic limits of lightweight laminated-structure as a protective panel for armoured vehicle. *Journal of Mechanical Engineering (JMEchE)*, 4(3), 20-34.
- [10]. Kılıç, N., Bedir, S., Erdik, A., Ekici, B., Taşdemirci, A., & Güden, M. (2014). Ballistic behavior of high hardness perforated armor plates against 7.62 mm armor piercing projectile. *Materials & Design*, 63, 427-438.
- [11]. Wang, K., Li, M., Yan, P., & Dong, L. (2022). An Experimental and Numerical Study on the Ballistic Performance of Multi-Layered Moderately-Thick Metallic Targets against 12.7-mm Projectiles. *CMES-Computer Modeling in Engineering & Sciences*, 131(1), 165-197.
- [12]. Giglio, M., Gilioli, A., Manes, A., Peroni, L., & Scapin, M. (2012). Investigation about the influence of the mechanical properties of lead core and brass jacket of a NATO 7.62 mm ball bullet in numerical simulations of ballistic impacts. *EPJ Web of Conferences*.
- [13]. Paris, V., Weiss, A., Vizek, A., Ran, E., & Aizik, F. (2012). Fragmentation of armor piercing steel projectiles upon oblique perforation of steel plates. In *EPJ Web of Conferences*, 26. EDP Sciences.
- [14]. Iqbal, M. A., Senthil, K., Sharma, P., & Gupta, N. K. (2016). An investigation of the constitutive behavior of ArmoX 500T steel and armor piercing incendiary projectile material. *International Journal of Impact Engineering*, 96, 146-164.
- [15]. Autodyn. (2005). AUTODYN explicit software for nonlinear dynamics. *Century Dynamics Inc.*
- [16]. Lesuer D. (1999). *Experimental investigations of material models for Ti-6Al-4V and 2024-T3*. Lawrence Livermore National Lab.
- [17]. Dey, S. A., Børvik, T., Hopperstad, O. S., Leinum, J. R., & Langseth, M. (2004). The effect of target strength on the perforation of steel plates using three different projectile nose shapes. *International Journal of Impact Engineering*, 30, 1005-1038.
- [18]. Buchar, J., Voldrich, J., Rolc, S., & Lisy, J. (2020). Ballistic performance of the dual hardness armour. *Proceedings of 20th International symposium on ballistics*. Orlando, FL.
- [19]. Iqbal, M. A., Senthil, K., Bhargava, P., & Gupta, N. K. (2015). The characterization and ballistic evaluation of mild steel. *International Journal of Impact Engineering*, 78, 98-113.
- [20]. Fras, T., Murzyn, A., & Pawlowski, P. (2017). Defeat mechanisms provided by slotted add-on bainitic plates against small-calibre 7.62 mm× 51 AP projectiles. *International Journal of Impact Engineering*, 103, 241-253.
- [21]. Burian, W., *et al.* (2019). Protection effectiveness of perforated plates made of high strength steel. *International Journal of Impact Engineering*, 126, 27-39.
- [22]. Nsiampa, N., Coghe, F., & Dyckmans, G. (2009). Numerical investigation of the bodywork effect (K-effect). In *Proceedings of the Ninth International Conference on the Mechanical and Physical behavior of Materials Under Dynamic Loading*, 1561-1566.

- [23]. Iqbal, M. A., Senthil, K., Sharma, P., & Gupta, N. K. (2016). An investigation of the constitutive behavior of Armox 500T steel and armor piercing incendiary projectile material. *International Journal of Impact Engineering*, 96, 146-164.
- [24]. Nilsson, M. (2003). Constitutive model for Armox 500T and Armox 600T at low and medium strain rates. *Swedish Defence Research Agency, Stockholm*.
- [25]. Hazell, P. J. (2022). *Armour: materials, theory, and design*. CRC press.
- [26]. Banerjee, A., Dhar, S., Acharyya, S., Datta, D., & Nayak, N. (2015). Determination of Johnson cook material and failure model constants and numerical modelling of Charpy impact test of armour steel. *Materials Science and Engineering: A*, 640, 200-209.
- [27]. ASM Aerospace Specification Metals. (n.d.). *Aluminum alloy 5083-H116 data*. ASM matweb. Retrieved from: <https://asm.matweb.com/search/SpecificMaterial.asp?bassnum=ma5083h116> [accessed: 10 June 2024].
- [28]. Iqbal, M. A., Diwakar, A., Rajput, A., & Gupta, N. K. (2012). Influence of projectile shape and incidence angle on the ballistic limit and failure mechanism of thick steel plates. *Theoretical and Applied Fracture Mechanics*, 62, 40-53.
- [29]. AZO Materials. (2020). *Titanium Alloy - Ti6Al4V Grade 5*. Azom. Retrieved from: <https://www.azom.com/properties.aspx?ArticleID=1547> [accessed: 12 June 2024].
- [30]. AZO Materials. (2020). *AISI 4340 Alloy Steel (UNS G43400)*. Azom. Retrieved from: <https://www.azom.com/article.aspx?ArticleID=6772> [accessed: 13 June 2024].
- [31]. MatWeb Material property data. (n.d.). *Home page*. Matweb. Retrieved from: https://www.matweb.com/search/DataSheet.aspx?MatGUID=57483b4d782940faaf12964a1821fb61&ckck=_1 [accessed: 15 June 2024].
- [32]. Børvik, T., *et al.* (2005). Strength and ductility of Weldox 460 E steel at high strain rates, elevated temperatures and various stress triaxialities. *Engineering fracture mechanics*, 72(7), 1071-1087.
- [33]. Forrestal, M. J., Børvik, T., & Warren, T. L. (2010). Perforation of 7075-T651 aluminum armor plates with 7.62 mm APM2 bullets. *Experimental Mechanics*, 50, 1245-1251.
- [34]. Foundry Lexicon.(n.d.). *ARMCO iron data*. *Giessereilexikon*. Retrieved from: <https://www.giessereilexikon.com/en/foundry-lexicon/Encyclopedia/show/armco-iron-4774/?cHash=308e1c40679f2eae0df3dbc68431cf2b> [accessed: 18 June 2024].